Supplementary Information for
Universal Dynamical Onset in Water at Distinct Material Interfaces

Lirong Zheng, Zhuo Liu, Qiang Zhang, Song Li, Juan Huang, Lei Zhang, Bing Zan, Madhusudan Tyagi, He Cheng, Taisen Zuo, Victoria García Sakai, Takeshi Yamada, Chenxing Yang, Pan Tan, Fan Jiang, Hao Chen, Wei Zhuang, Liang Hong

Email: Liang Hong, hongl3liang@sjtu.edu.cn.

Wei Zhuang, wzhuang@fjirsm.ac.cn.

Qiang Zhang, qzhang@imun.edu.cn.

He Cheng, chenghe@ihep.ac.cn.

This PDF file includes:

Methods

Sample preparation.

Lysozyme (LYS) from chicken egg white was purchased from Sigma Aldrich (Shanghai, China), and Creatine Amidinohydrolas (CK) was supplied from Prof. Guangyu Yang (School of Life Sciences and Biotechnology, Shanghai Jiao Tong University, Shanghai, China). The expression and purification of hydrogenated and perdeuterated cytochrome P450 (CYP) and Green Fluorescent Protein (GFP) are described previously (*1-4*). In order to exclude the effect of ions, the proteins were dialyzed before experiments. For simplification, the regular proteins and its perdeuterated counterparts are denoted as H-proteins and D-proteins in the manuscript, respectively. All the H-proteins were dissolved in D_2O to allow full deuterium exchange of all exchangeable hydrogen atoms and then lyophilized for 12 hours to obtain the dry sample. The lyophilized H-protein is then put into a desiccator with D_2O, placed in the glove box purged with nitrogen gas, to absorb D_2O till the desired hydration level, h (gram water/gram protein). In contrast, the preparation of the deuterated proteins was conducted in the opposite way. The D-proteins were dissolved in H_2O to allow full hydrogen exchange and then lyophilized for 12 hours. The lyophilized D-protein was then put into a desiccator with H_2O to absorb H_2O till the desired h. The ultrapure water (H_2O) was supplied by a Millipore Direct-Q system (18.2 MΩ·cm at 25 °C), whereas the deuterium oxidized (D_2O, 99.9 atom % D) was purchased from Sigma-Aldrich (Shanghai, China). The hydration levels of protein samples were controlled by measuring the sample weights before and after water adsorption. In this work, h ranges from 0.2, 0.3 and 0.4. The accuracy of h is controlled within 10% error. E.g., h = 0.4±0.04 gram water/gram protein. The tRNA and DNA were purchased from Sigma Aldrich (Shanghai, China). The hydrogenated and perdeuterated ethylene oxide, purchased from Cambridge Isotope Laboratories, Inc. (Andover, MA, US), were used to synthesize the hydrogenated polyethylene glycol (H-PEG) and perdeuterated polyethylene glycol (D-PEG), respectively. The molecular weight (M_w) of PEG is 2400 g/mol. The hydration process on tRNA, DNA and PEG is the same as that of protein. The hydration level of tRNA, DNA and PEG is h = 0.5, 0.5, and 0.3, respectively.

The rGO powder sample was purchased from Nanjing XFNANO Materials Tech Co. Ltd., China, which was thermally reduced from GO prepared by a modified Hummers' method (*5*). The GOM (membrane) samples were synthesized by following modified Hummers' method (*5*), whose oxidation rate is determined by X-ray photoelectron spectroscopy (XPS) as 28%. The hydration

process on rGO and GOM is the same as that for D-protein. Final h obtained were: 0.1, 0.2 and 0.9 for rGO and 0.4 and 0.9 for GOM.

All samples were sealed tightly in the aluminum cans in nitrogen before the neutron scattering experiments.

Elastic incoherent neutron scattering (EINS).

The elastic scattering intensity $S(q, \Delta t)$ is normalized to the lowest temperature and is approximately the value of the intermediate scattering function when decaying to the instrument resolution time, Δt. $S(q, \Delta t)$ was obtained in the temperature range from 10 K (or 100 K) to 300 K during heating process with the rate of 1.0 K/min by using the HFBS at NIST, OSIRIS at ISIS and DNA at J-PARC. The instrumental energy resolutions are 1 μeV (HFBS), 13 μeV (DNA), 25.4 μeV and 99 μeV (OSIRIS in two different configurations), corresponding to timescales of 1 ns (*6*), 80 ps (*7, 8*), 40 ps (*9*) and 10 ps (*9*), respectively. The results from instruments with various resolutions were summed over the same q from 0.45 to 1.75 $Å^{-1}$.

Gaussian approximation.

At 150 and 200 K, the Gaussian approximation holds approximately valid, where $\log(S(q, \Delta t))$ depends linearly on q^2 over the whole q-range measured (0.45-1.75 $Å^{-1}$) (see Fig. S1), indicating harmonic motions of the hydration water. Above 200 K, however, the Gaussian approximation fails significantly: $\log(S(q, \Delta t))$ is no longer a linear function of q^2 at 0.45-1.75 $Å^{-1}$, indicating that anharmonic motions are set in. Such analysis supports our findings by examining the temperature dependence of elastic intensity that the dynamical onset temperature is ~ 200 K.

In order to calculate the mean-square displacements (MSD) of surface water derived from Gaussian approximation at different temperatures, we extracted MSD in the q-range from 0.45-0.87 $Å^{-1}$. The Gaussian application holds valid in this q range for the entire temperature window studied (10 to 290 K). As can be seen in Fig. S2, the onset temperature (T_{on}) of hydration water is ~200 K across different materials as measured by the temperature dependence of MSD, which is coincident with the results obtained from the temperature dependence of the dynamical structure factor $S(q, \Delta t)$ in Fig. 1a.

Molecular dynamics (MD) simulations.

The initial structure of protein cytochrome P450 (CYP) for simulations was taken from PDB crystal structure (1dz9) (*10*). Two protein monomers were filled in cubic box (see Fig. 4a). 2025 water molecules were inserted into box randomly to reach a mass ratio of 0.4 gram water/1 gram

protein, which mimics the experimental condition. Then 34 sodium counter ions were added to keep the system neutral in charge. The CHARMM 27 force field in GROMACS package was used for CYP, whereas the TIP4P/Ew model was chosen for water (*11*). The simulations were carried out at a broad range of temperatures from 360 K to 100 K, with a step of 5 K, to study the temperature-dependent properties. At each temperature, after the 5000 steps energy-minimization procedure, a 10 ns NVT is conducted. After that, a 30 ns NPT simulation was carried out at 1 atm with the proper periodic boundary condition. The temperature and pressure of system is controlled by the velocity rescaling method (*12*) and the method by Parrinello and Rahman (*13*), respectively. All bonds of water in all the simulations were constrained with the LINCS algorithm to maintain their equilibration length (*14*). In all the simulations, the system was propagated using the leap-frog integration algorithm (*15*) with a time step of 2 fs. The electrostatic interactions were calculated using the Particle Mesh Ewalds (PME) (*16*) method. A non-bond pair-list cutoff of 1 nm was used and the pair-list was updated every 20 fs.

We also performed MD simulation on hydrated GOM system at different temperatures, with the mass ratio of 0.4 gram water/1 gram GOM to mimic the experimental condition. We used the OPLS-AA force field for GOM, and TIP4P/Ew for water (*11*). The interaction model between GOM and water are derived based on the combination rule (*17*). The simulation cell contains two layers of GO, and is periodically repeated in all dimensions (see Fig. 4d). The GO sheets contain 960 carbon atoms, 110 hydroxyl groups and 96 epoxy groups (*18, 19*). The distribution of oxidized groups was determined based on the rate constant of the oxidation reaction. The oxidation reaction pathways and corresponding energy barrier were calculated using DFT. Then the calculated energy barrier was used to derive the rate constant based on the conventional transition state theory (*20*). The net oxidation rate is 23%, mimicking the experimental sample (28%) as determined by XPS. The simulation procedures adopted are the same as those used in the CYP systems.

All MD simulations were performed using GROMACS 4.5.1 (*21, 22*) (CYP) and LAMMPS (*23*) (GOM) software packages. Representative simulation snapshots of the two systems are given in Figs. 4a and 4d, respectively.

We analyzed the MD results on four samples (CYP, GOM, tRNA and DNA) and illustrated the water coverage in Fig. S13, where ~86-90% of the substrate surface is covered by water at $h = 0.4$ gram water/gram substrate materials. Moreover, as shown in Fig. S14, the hydration level studied in these four samples correspond to the case that ~85-95% of surface water stays in the first

hydration shell and ~5%-15% of surface water stays in the second hydration shell. Hence, the majority of hydration water stays within the first hydration shell of substrates.

Deriving neutron spectra from MD trajectories.

The neutron spectra were derived from MD simulations by calculating the incoherent intermediate scattering function, $I(q, t)$:

$$I(q, t) = \frac{1}{N}\sum_{j}^{N} b_j{}^2 \left\langle exp[-i\vec{q}\vec{R}_j(t_0)] exp[i\vec{q}\vec{R}_j(t_0 + t)] \right\rangle_{t_0} \quad \text{(S1)}$$

where $\vec{q}$ is the scattering wave vector, N is the total number of atoms, b_j is the incoherent scattering length of a given atom j, a fundamental constant to characterize the interaction between the element and neutron, which was tabulated in Ref. (*24*), $\vec{R}_j(t_0)$ is the time dependent position vector of that atom, and the brackets denote the orientational average. The MD-derived $S(q, \Delta t)$ is approximated as the value of $I(q, t)$ when $t = \Delta t$ (*25, 26*).

The hydrogen bond correlation function.

Two water molecules are considered to be hydrogen bonded if the two distances $R_{O^*O^a} < 3.1$ Å, $R_{H^*O^a} < 2.0$ Å and the angle $\theta_{H^*O^*O^a} < 20^o$ (*27, 28*). H* and O* are the hydrogen and oxygen atoms from the hydrogen-bond donor water. O^a denotes the oxygen in the hydrogen bond acceptor water.

We herein computed the hydrogen bond exchange rate constant by calculating a cross correlation function in the stable states picture (SSP) (*27, 29, 30*). A specific hydrogen bond switching event begins with the stable hydrogen bond reactant state of O*-H*⋯O^a and ends with the stable product state O*-H*⋯O^b (O^b denotes the oxygen in the final hydrogen bond acceptor water). The cross-correlation function is then defined as (*27, 29, 30*):

$$C_H(t) = 1 - \langle n_R(0) n_p(t) \rangle \quad \text{(S2)}$$

The hydrogen bond state functions $n_R(t) = 1$ at the stable reactant state and $n_R(t) = 0$ otherwise. $n_P(t) = 1$ at the stable product state and $n_P(t) = 0$ otherwise. $C_H(t)$ represents a forming probability of a stable product at time t, when the system is in the reactant state at $t = 0$.

The characteristic relaxation time of the hydrogen-bond relaxation, i.e., switching of the hydrogen bond, is defined as the time when $C_H(t)$ decays to 1/e.

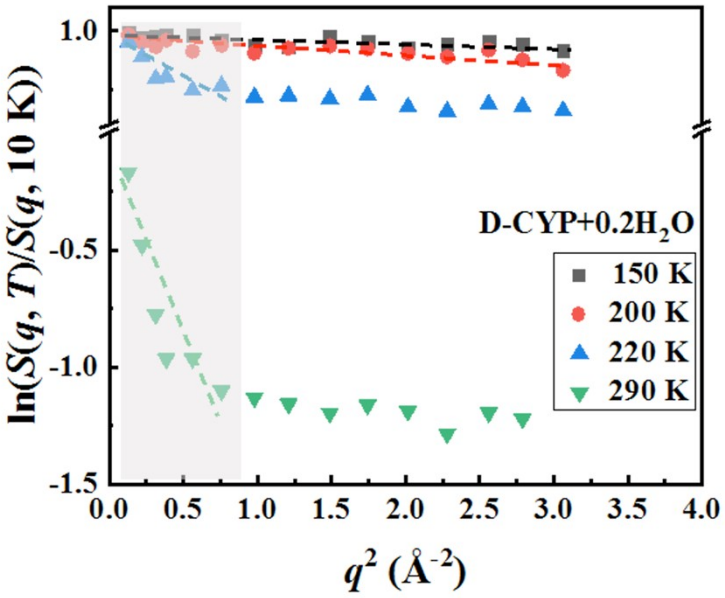

Fig. S1. log($S(q, \Delta t)$) versus q^2 plots of D-CYP hydrated in H_2O at different temperatures. The dashed lines show the linear q-range of hydration water at different temperatures. The transparent gray area is used to extract MSD in the q-range from 0.45-0.87 $Å^{-1}$.

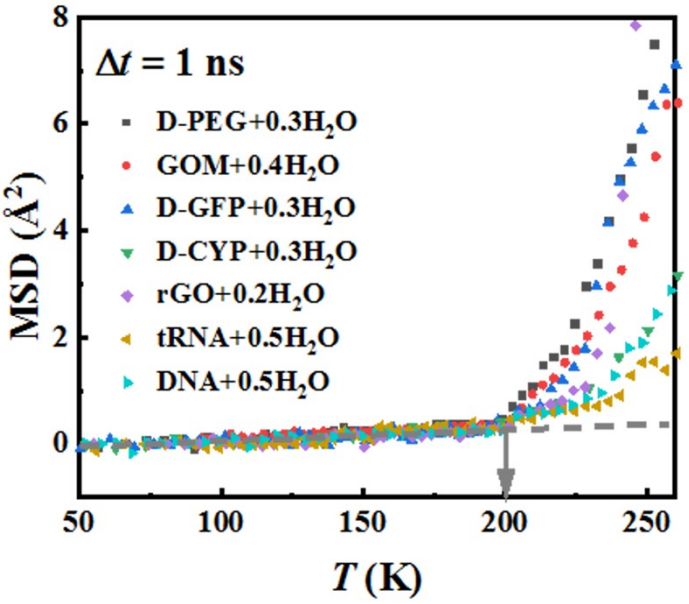

Fig. S2. MSD of the hydration water at distinct substrate materials. The MSD was extracted from the Gaussian approximation fitted between q values of 0.45 to 0.87 Å^{-1}. The gray arrow indicates the dynamical onset temperature of hydration water.

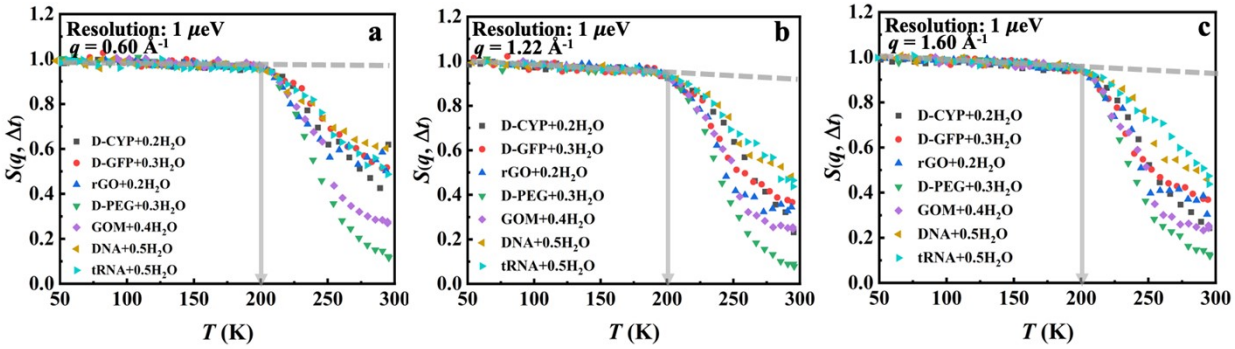

Fig. S3. Dynamical onset in hydration water as measured by HFBS at a resolution of 1 μeV (Δ*t* = 1 ns). The temperature-dependent elastic intensity $S(q, \Delta t)$ of the materials (tRNA, DNA, GOM, rGO, D-CYP, D-GFP and D-PEG) hydrated in H_2O at **(a)** q = 0.6, **(b)** 1.22 and **(c)** 1.6 $Å^{-1}$.

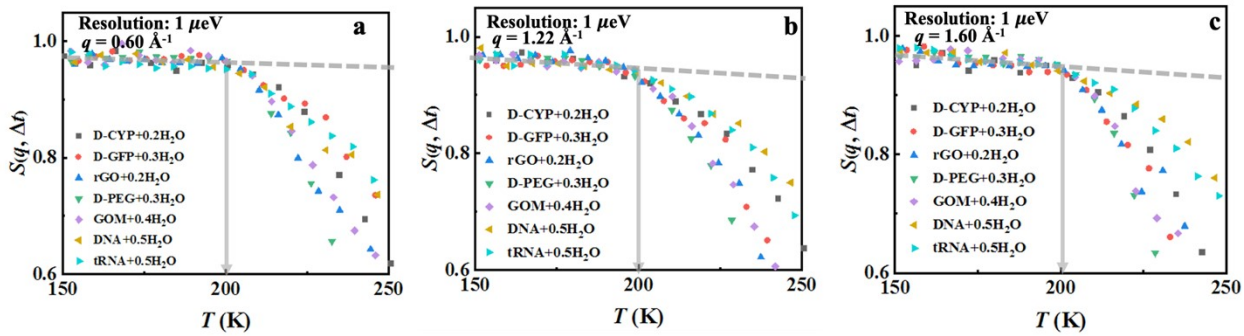

Fig. S4. The enlarged views from Fig. S3 showing the temperature of dynamical onset in hydration water.

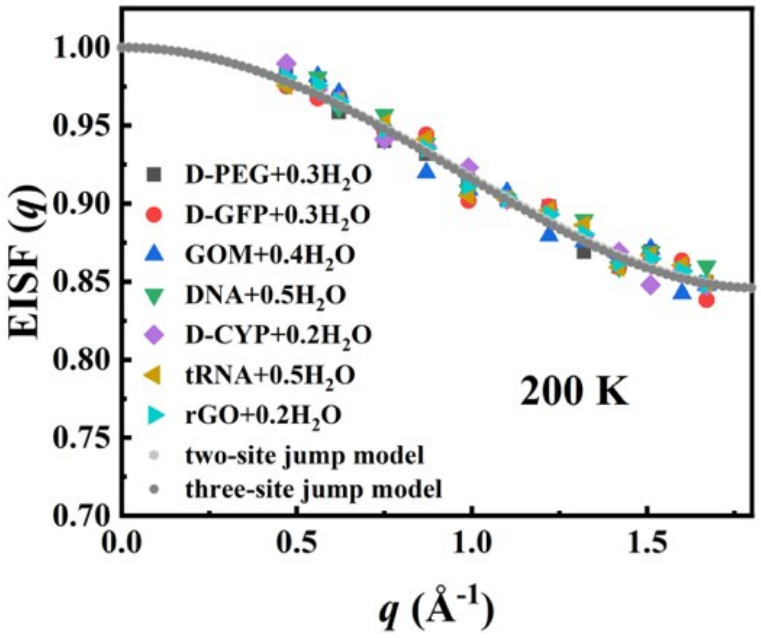

Fig. S5. EISF(q) of hydration water on distinct surface of substrates at dynamical onset temperature, ~200 K, as measured by HFBS at a resolution of 1 μeV (Δt = 1 ns). The light gray line and dark gray line present fit to the two-site and three-site jump models, respectively. The fits of two-site and three-site jump model are indistinguishable at this q-range.

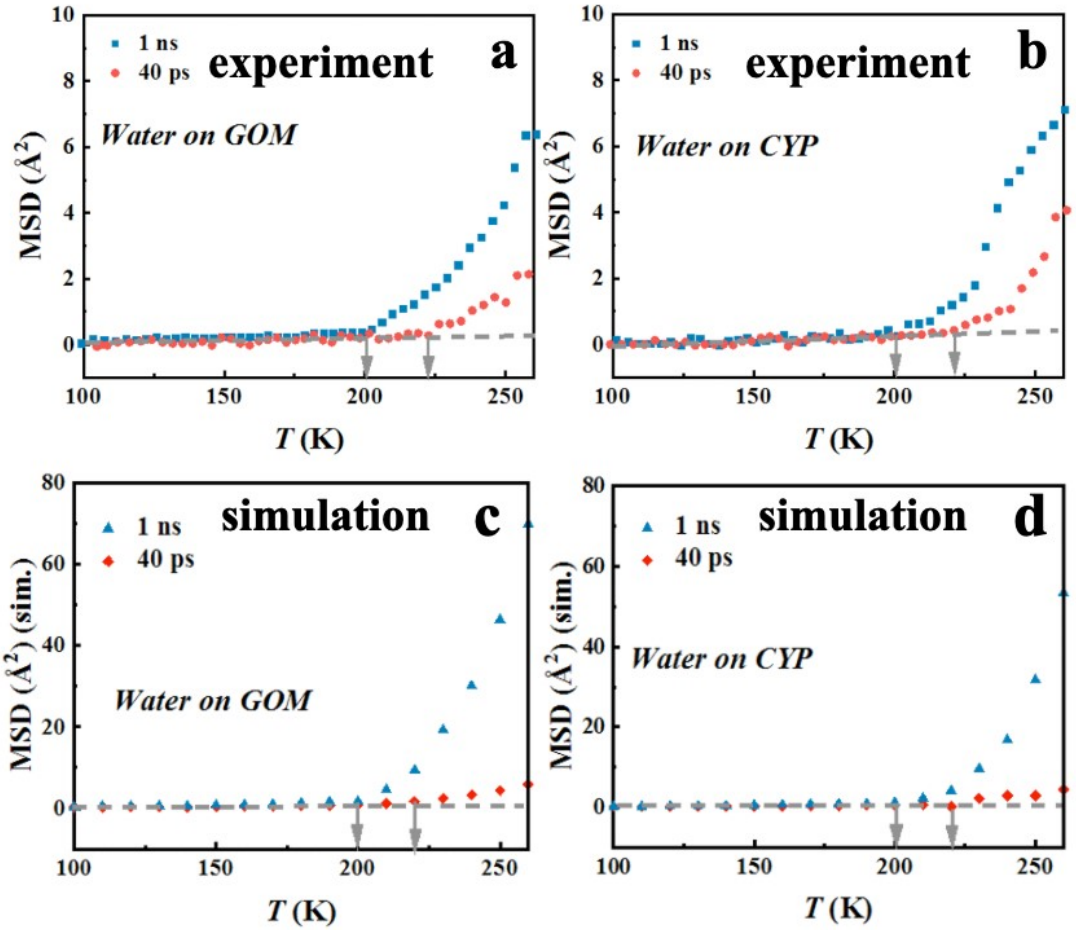

Fig. S6. Dynamical onset of hydration water obtained from neutron scattering and MD simulation at different resolutions. MSD of hydration water **(a, c)** at the surface of GOM and **(b, d)** at the surface of CYP obtained from experiments and simulations.

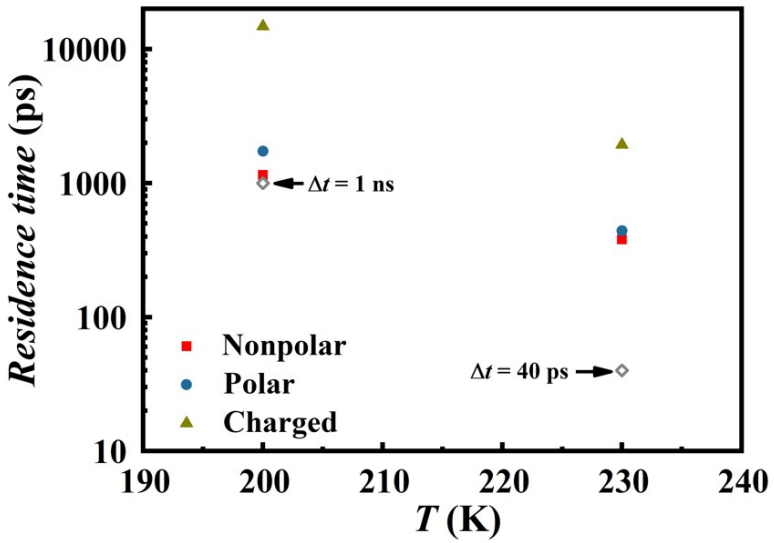

Fig. S7. Residence time of water molecules around specific types of residue on CYP surface obtained from MD. Here, two temperatures 200 and 230 K were chosen as they are the corresponding T_{on} for Δt = 1 ns and 40 ps, respectively.

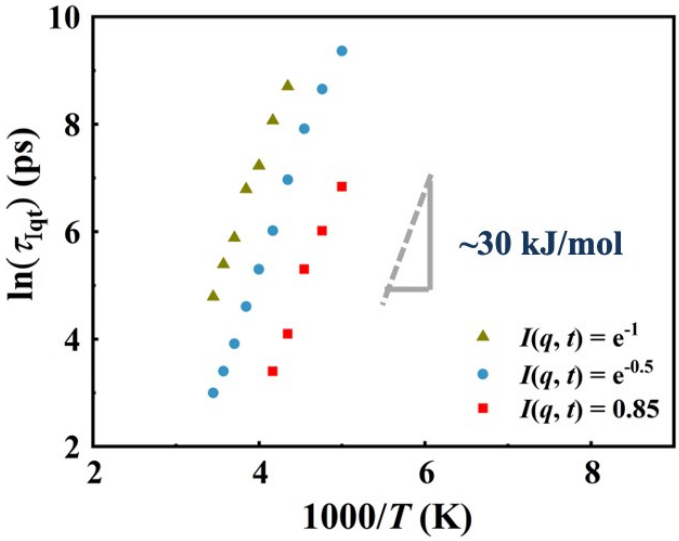

Fig. S8. The characteristic relaxation time, τ_{lqt}, of water on the protein as a function of inverse temperature. Here, τ_{lqt} is defined as the time when the corresponding $I(q, t)$ decays to 0.85, $e^{-0.5}$ and e^{-1} at q = 1 Å^{-1}, respectively. The average q value is explored experimentally. As can be seen, although the choice of the value of $I(q, t)$ will affect the absolute value of τ_{lqt}, it will not alter much the corresponding energy barrier. In the present work, the value of 0.85 is chosen for analysis in the main text, as this value mimics the experimental data around T_{on}.

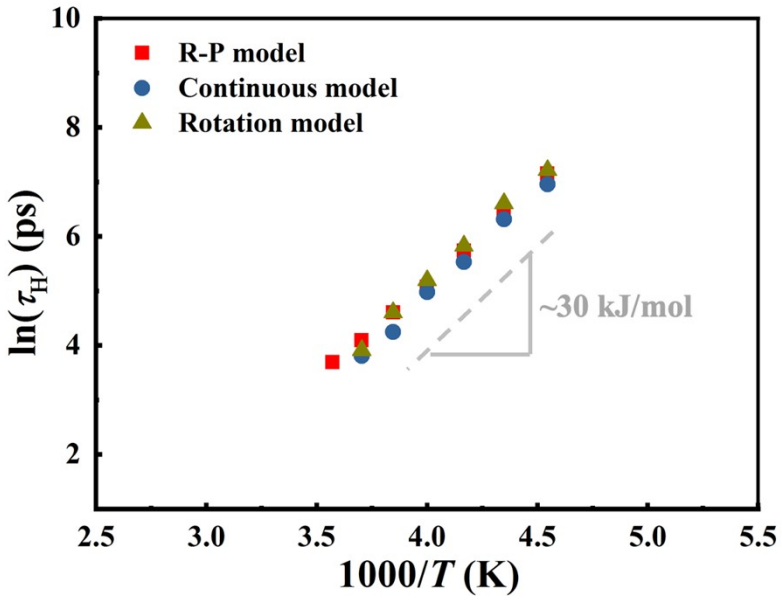

Fig. S9. Dynamics of the water-water hydrogen bond relaxation by different definition of hydrogen bond derived from MD. The characteristic relaxation time, τ_H, of water-water hydrogen bond as a function of inverse temperature. Continuous model and rotation model are referenced from Ref. (*31*) and Ref. (*32*), respectively. R-P model is used in the main text.

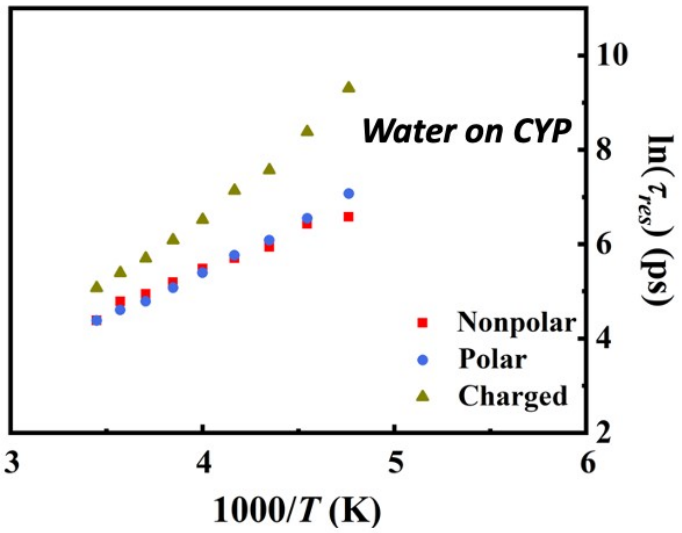

Fig. S10. Temperature dependence of the residence time (τ_{res}) of water around various types of residues on CYP derived from MD.

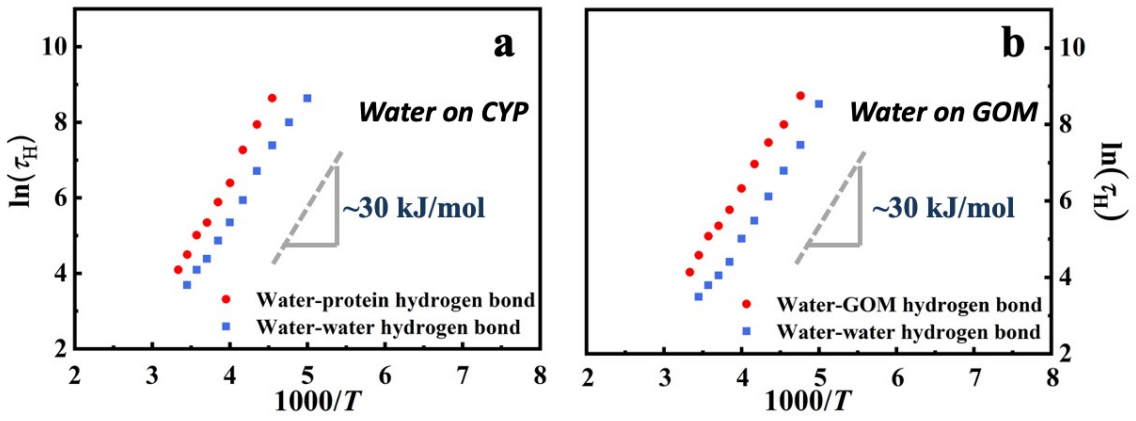

Fig. S11. Dynamics of the hydrogen bond relaxation derived from MD. The characteristic relaxation time, τ_H, of **(a)** water-water and water-protein hydrogen bond as a function of inverse temperature on CYP and **(b)** water-water and water-GOM hydrogen bond as a function of inverse temperature on GOM.

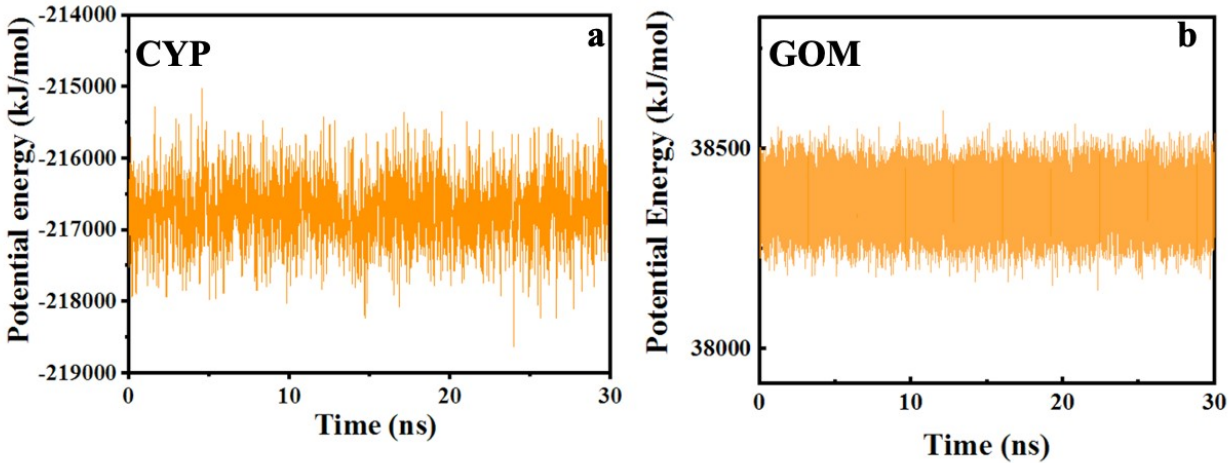

Fig. S12. The potential energy as a function of MD trajectory time of (a) CYP and (b) GOM.

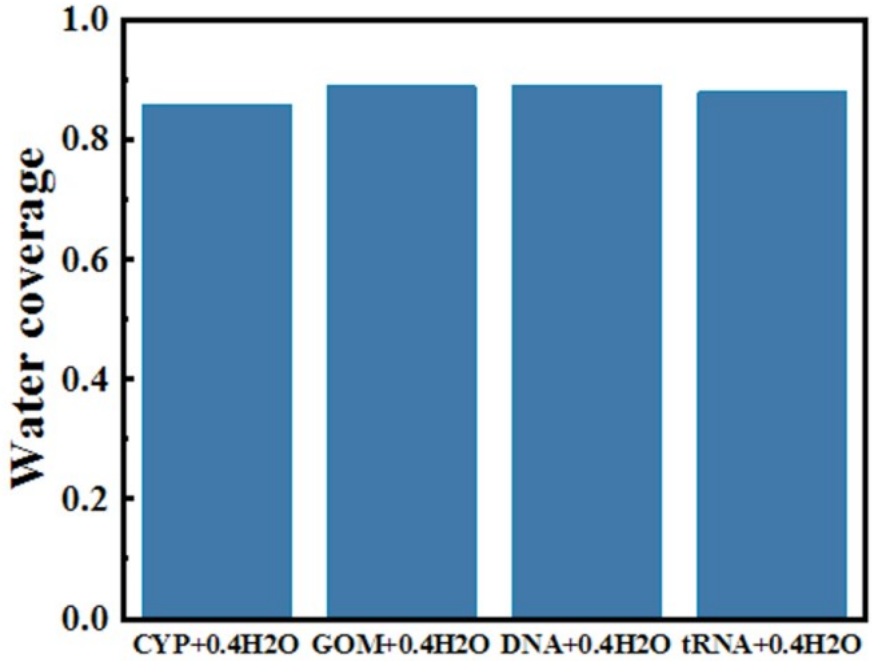

Fig. S13. The water coverage of CYP, GOM, tRNA and DNA system. The definition of water coverage is the ratio of the surface area reached by hydration water to the total surface area of substrate materials.

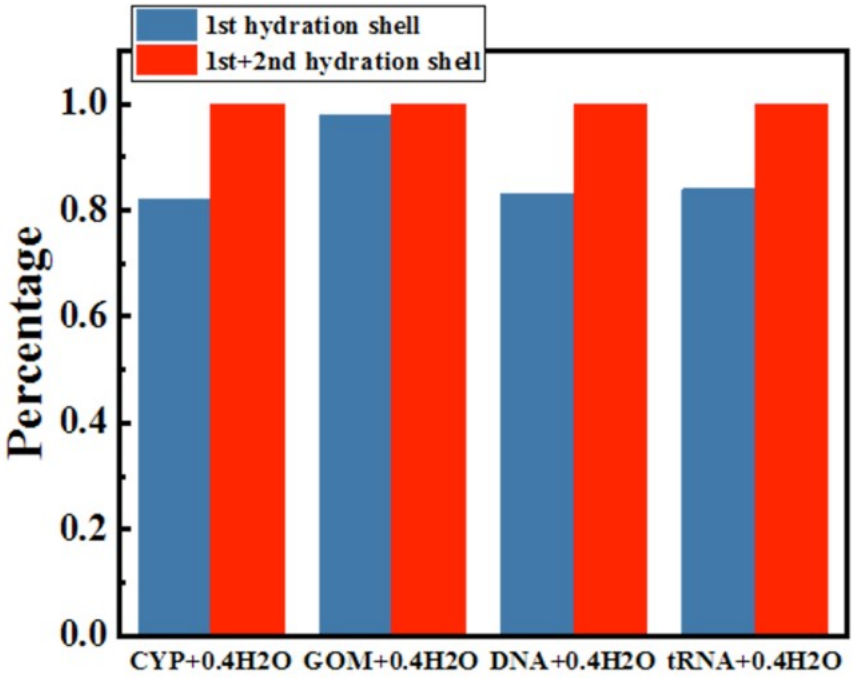

Fig. S14. The ratio of water within first hydration shell and second hydration shell in CYP, GOM, tRNA and DNA system. The definition of the hydration shell is referenced by Ref. (PNAS, 2002, 99, 5478-5383.).

Table S1. Dynamical onset temperatures of various materials themselves measured by HFBS at NIST or IN16 at ILL (Δt = 1 ns)

Materials	T_{on}
Lipid membrane	260 K (*33*)
DNA	225 K (*34*)
tRNA	200 K (*35*)
LYS	213 K
PEG	230 K
CK	250 K

Table S2. Relative contributions from the materials and their hydration water to the neutron scattering signals in each sample presented in Fig. 1a and 1b in the main text

	Hydrated materials	Signals from materials	Signals from hydration water
Fig. 1a	DNA+0.5H_2O	43%	57%
	tRNA+0.5H_2O	43%	57%
	D-CYP+0.2H_2O	34%	66%
	D-GFP+0.3H_2O	25%	75%
	rGO+0.2H_2O	20%	80%
	GOM+0.4H_2O	10%	90%
	D-PEG+0.3H_2O	28%	72%
Fig. 1b	tRNA+0.59D_2O	81%	19%
	H-LYS+0.3D_2O	95%	5%
	H-PEG+0.3D_2O	96%	4%
	H-CK+0.3D_2O	96%	4%

References

1. Liu, Z. *et al.* Dynamical Transition of Collective Motions in Dry Proteins. *Phys. Rev. Lett.* 119, 048101 (2017).
2. Nickels, J. D. *et al.* Dynamics of Protein and its Hydration Water: Neutron Scattering Studies on Fully Deuterated GFP. *Biophys. J.* 103, 1566-1575 (2012).
3. Miao, Y. *et al.* Coupled flexibility change in cytochrome P450cam substrate binding determined by neutron scattering, NMR, and molecular dynamics simulation. *Biophys. J.* 103, 2167-2176 (2012).
4. Meilleur, F., Dauvergne, M. T., Schlichting, I. & Myles, D. Production and X-ray crystallographic analysis of fully deuterated cytochrome P450cam. *Acta Crystallogr. D.* 61, 539-544 (2005).
5. Hummers, W. S. & Offeman, R. E. Preparation of Graphitic Oxide. *J. Am. Chem. Soc.* 80, 1339-1339 (1958).
6. Meyer, A., Dimeo, R. M., Gehring, P. M. & Neumann, D. A. The high-flux backscattering spectrometer at the NIST Center for Neutron Research. *Rev. Sci. Instrum.* 74, 2759-2777 (2003).
7. Fujiwara, S. *et al.* Ligation-Dependent Picosecond Dynamics in Human Hemoglobin As Revealed by Quasielastic Neutron Scattering. *J. Phys. Chem. B* 121, 8069-8077 (2017).
8. Fujiwara, S. *et al.* Dynamical Behavior of Human α-Synuclein Studied by Quasielastic Neutron Scattering. *PLOS ONE* 11, e0151447 (2016).
9. Telling, M. T. F. & Andersen, K. H. Spectroscopic characteristics of the OSIRIS near-backscattering crystal analyser spectrometer on the ISIS pulsed neutron source. *Phys. Chem. Chem. Phys.* 7, 1255-1261 (2005).
10. Schlichting, I. *et al.* The Catalytic Pathway of Cytochrome P450cam at Atomic Resolution. *Science* 287, 1615-1622 (2000).
11. Horn, H. W. *et al.* Development of an improved four-site water model for biomolecular simulations: TIP4P-Ew. *J. Chem. Phys.* 120, 9665-9678 (2004).
12. Bussi, G., Donadio, D. & Parrinello, M. Canonical sampling through velocity rescaling. *J. Chem. Phys.* 126, 014101 (2007).
13. Parrinello, M. & Rahman, A. Polymorphic transitions in single crystals: A new molecular dynamics method. *J. Appl. Phys.* 52, 7182-7190 (1981).
14. Hess, B., Bekker, H., Berendsen, H. J. C. & Fraaije, J. G. E. M. LINCS: A linear constraint solver for molecular simulations. *J. Comput. Chem.* 18, 1463-1472 (1997).
15. Miyamoto, S. & Kollman, P. A. Settle: An analytical version of the SHAKE and RATTLE algorithm for rigid water models. *J. Comput. Chem.* 13, 952-962 (1992).
16. Darden, T., York, D. & Pedersen, L. Particle mesh Ewald: An N·log(N). method for Ewald sums in large systems. *J. Chem. Phys.* 98, 10089-10092 (1993).
17. Robertson, M. J., Tirado-Rives, J. & Jorgensen, W. L. Improved Peptide and Protein Torsional Energetics with the OPLS-AA Force Field. *J. Chem. Theory Comput.* 11, 3499-3509 (2015).
18. Shih, C.-J., Lin, S., Sharma, R., Strano, M. S. & Blankschtein, D. Understanding the pH-Dependent Behavior of Graphene Oxide Aqueous Solutions: A Comparative Experimental and Molecular Dynamics Simulation Study. *Langmuir* 28, 235-241 (2012).
19. Medhekar, N. V., Ramasubramaniam, A., Ruoff, R. S. & Shenoy, V. B. Hydrogen Bond Networks in Graphene Oxide Composite Paper: Structure and Mechanical Properties. *ACS Nano* 4, 2300-2306 (2010).

20. Liu, Z. *et al.* Heterogeneity of Water Molecules on the Free Surface of Thin Reduced Graphene Oxide Sheets. *J. Phys. Chem. C* 124, 11064-11074 (2020).
21. Berendsen, H. J. C., van der Spoel, D. & van Drunen, R. GROMACS: A message-passing parallel molecular dynamics implementation. *Comput. Phys. Comm.* 91, 43-56 (1995).
22. Lindahl, E., Hess, B. & van der Spoel, D. GROMACS 3.0: a package for molecular simulation and trajectory analysis. *J. Mol. Model* 7, 306-317 (2001).
23. Plimpton, S. Fast Parallel Algorithms for Short-Range Molecular Dynamics. *J. Comput. Phys.* 117, 1-19 (1995).
24. Sears, V. F. Neutron scattering lengths and cross sections. *Neutron News* 3, 26-37 (1992).
25. Hong, L. *et al.* Elastic and Conformational Softness of a Globular Protein. *Phys. Rev. Lett.* 110, 028104 (2013).
26. Doster, W. The two-step scenario of the protein dynamical transition. *J. Non-Cryst. Solids* 357, 622-628 (2011).
27. Laage, D. & Hynes, J. T. A Molecular Jump Mechanism of Water Reorientation. *Science* 311, 832-835 (2006).
28. Laage, D. & Hynes, J. T. On the Molecular Mechanism of Water Reorientation. *J. Phys. Chem. B* 112, 14230-14242 (2008).
29. Zhang, Q., Wu, T., Chen, C., Mukamel, S. & Zhuang, W. Molecular mechanism of water reorientational slowing down in concentrated ionic solutions. *Proc. Nat. Acad. Sci.* 114, 10023-10028 (2017).
30. Zhang, Q. *et al.* The opposite effects of sodium and potassium cations on water dynamics. *Chem. Sci.* 8, 1429-1435 (2017).
31. Luzar, A., Chandler, D. Hydrogen-bond kinetics in liquid water. *Nature* **379**, 55-57 (1996).
32. Tay, K. A., Bresme, F. Kinetics of hydrogen-bond rearrangements in bulk water. *Phys. Chem. Chem. Phys.* 11, 409-415 (2009).
33. Wood, K. *et al.* Coupling of protein and hydration-water dynamics in biological membranes. *Proc. Nat. Acad. Sci.* 104, 18049-18054 (2007).
34. Chen, S. H. *et al.* Experimental evidence of fragile-to-strong dynamic crossover in DNA hydration water. *J. Chem. Phys.* 125, 171103 (2006).
35. Caliskan, G. *et al.* Dynamic Transition in tRNA is Solvent Induced. *J. Am. Chem. Soc.* 128, 32-33 (2006).